Ionics (2013) 19:1155–1162
DOI 10.1007/s11581-012-0834-5

ORIGINAL PAPER

Effect of Co substitution for Fe in Sr_2FeMoO_6 on electrocatalytic properties for oxygen reduction in alkaline medium

Mabrouk Cheriti · Abdelkrim Kahoul · Amor Azizi · Nicolas Alonso-Vante

Received: 9 September 2012 / Revised: 11 November 2012 / Accepted: 25 November 2012 / Published online: 12 December 2012

Abstract Double perovskites $Sr_2Fe_{1-x}Co_xMoO_6$ (x=0, 0.25, 0.5, 0.75 and 1) have been investigated as cathode material for oxygen reduction reaction (ORR) in 0.5 M NaOH at 25 °C using the rotating disk electrode. The electrocatalytic powders were prepared by a solid-state process and characterised by X-Ray powder diffraction, scanning electron microscopy and infrared spectroscopy. The electrochemical techniques considered are linear voltammetry, steady-state polarization and impedance spectroscopy. The electrocatalysts $Sr_2Fe_{1-x}Co_x$ MoO_6/C consisting of the double perovskite oxides and carbon (Vulcan XC-72) were mixed and spread out into a thin layer on a glassy carbon substrate. The electrocatalytic activity was strongly influenced by the Co substitution at room temperature. The relation between catalytic performance and the degree of Co content was examined. The Co-containing catalysts exhibited lower activity attributed to their high resistivity, and the highest activity toward oxygen reduction was observed for Sr_2CoMoO_6.

Keywords Double perovskite · Oxygen reduction · Rotating disk electrode · Electrochemical measurements

M. Cheriti · A. Kahoul (✉)
Laboratoire d'Energétique et d'Electrochimie des Solides,
Université F. Abbas de Sétif, 19000 Sétif, Algeria
e-mail: kahoulabdelkrim@yahoo.fr

A. Azizi
Laboratoire de Chimie, Ingénierie Moléculaire et Nanostructures,
Université F. Abbas de Sétif, 19000 Sétif, Algeria

N. Alonso-Vante
Laboratoire de Catalyse en Chimie Organique, UMR CNRS 6503,
Université de Poitiers, 4 rue Michel Brunet, B27-BP633,
86022 Poitiers, France

Introduction

The electrochemical oxygen reduction reaction (ORR) is of special importance due to its central role in many fields, such as energy conversion (metal air batteries, alkaline fuel cells), electrosynthesis of hydrogen peroxide and galvanic sensor for dissolved oxygen. Oxygen reduction on perovskite-structured oxides has attracted considerable attention since the work of Meadowcroft [1]. Many researchers have examined O_2 reduction and focused their interest on perovskite-type oxides ABO_3 (A = La, Ca or Sr and B = Co, Fe or Mn) [2–5]. Mixed with high surface area carbons, the perovskites exhibit excellent cathodic oxygen reduction properties in alkaline electrolytes. The activity of these oxide electrocatalysts can be correlated with either their highly active surfaces or the ability of the B cations to adopt different valency states, particularly when they form redox couples at the potential of oxygen reduction or evolution [6].

A subclass of perovskite oxides presented by the general formula $A_2BB'O_6$, known as "double perovskites", where A is an alkaline-earth atom such as (Sr, Ba or Ca) and B and B′ are transition-metal atoms. The ideal structure of these transition metal oxides can be viewed as a regular arrangement of corner-sharing BO_6 and $B'O_6$ octahedra, alternating along the directions of the crystal. This specific arrangement of alternating different B and B′ cations can be of great interest from the catalytic point of view since the properties of perovskites as electrocatalysts are generally determined by the nature, oxidation states and relative arrangement of B-site cations [7]. In order to optimize the physical properties of Sr_2FeMoO_6, such as electrical, magnetic and transport properties, a great deal of investigations on cationic partial substitution at Fe sites with some transition metals has been reported [8, 9]. This substitution is associated with an increased disorder in Fe/Mo sublattice of Sr_2FeMoO_6, leading to a reduction of the saturation magnetization M_s [10] and to

an increase of the electrical resistivity [11]. In our previous study [12], the ORR was investigated on Sr_2MMoO_6 (M = Fe and Co) double perovskites, prepared by a solid-state reaction, in 0.5 M NaOH at 25 °C with a rotating disk electrode (RDE). The two oxide powders (Sr_2FeMoO_6/C, Sr_2CoMoO_6/C) consisting of the double perovskite oxides and carbon (Vulcan XC-72) showed a significantly electrocatalytic activity for oxygen reduction. Compared to Sr_2FeMoO_6/C, the Sr_2CoMoO_6/C electrocatalyst was found to show a relatively high activity.

The purpose of this work is to extend the previous investigation in order to show the influence of Fe doping by replacing partial Fe ions with Co ones in $Sr_2Fe_{1-x}Co_xMoO_6$ (SFCMO) oxides on the ORR. Although much progress has been made on applications related to other areas for Sr_2MMoO_6 (M = Fe, Co), very little study has been undertaken on electrochemical properties of double perovskite oxides as oxygen electrode. Recently, it has been reported that some double perovskites used as anode [13] and cathode materials [14] displayed excellent electrochemical performances for the solid oxide fuel cells operating at high temperature. As per our knowledge, the electrochemical activity of these compounds has not been explored as oxygen electrode material in aqueous environment.

We report in this work the results concerning the structural, magnetic and electric properties of $Sr_2Fe_{1-x}Co_xMoO_6$ double perovskites and investigate the electrochemical behaviour of such compounds prepared as cathode materials for O_2 reduction reaction (ORR).

Experimental

Sample preparation

The $Sr_2Fe_{1-x}Co_xMoO_6$ (x in mole % is equal to 0, 0.25, 0.5 and 1) samples have been prepared by solid-state reaction using a high-purity $SrCO_3$, $Fe(C_2O_4).2H_2O$, CoO and MoO_3 as starting materials. A two-step process was adopted in order to avoid as much as possible the formation of $SrMoO_4$ [15], phase observed when all three compounds react within at one-step reaction [16]. First, appropriate stoichiometric amounts of $SrCO_3$, CoO and Fe $(C_2O_4).2H_2O$ were mixed, ground together and sintered in air at 1,000 °C. In the second step, the resulting powders ($Sr_2Fe_{1-x}Co_xO_{3+(1-x)/2}$) were mixed with MoO_3 and calcined at 1,150 °C during 2 h in a reducing atmosphere, a stream of N_2/H_2 (95:5). In all cases, the temperature increase was of 20 °C/min in order to limit the time period during which $SrMoO_4$ can be easily formed (between 600 and 900 °C). The samples were then slowly cooled at 5 °C/min down to room temperature under the reducing flow.

Procedures

As described previously [12], all electrochemical experiments were performed at (25±0.5 °C) using a thermostated three-electrode cell in 0.5 M NaOH electrolyte solution. The counter electrode used was a Pt plate with a large surface area. Potentials, in this article, are reported vs. an Hg/HgO reference electrode. The working electrode was a glassy carbon disk with 3.0 mm diameter. Carbon (Vulcan XC-72) supported double perovskites, and SFCMO were used as an electrocatalyst for oxygen reduction. Inks of the dispersed electrocatalysts SFCMO were made by mixing 3.4 mg oxide powder and 8 mg carbon with 250 μL Nafion® solution (5 % in mixture of lower aliphatic alcohols and water, Aldrich) and 1,250 μL ultrapure water (18 MΩcm) in an ultrasonic bath for 2 h. After polishing the glassy carbon disc with alumina Al_2O_3 powder (5 Å) and to immobilise oxide/XC-72, a 3-μL aliquot of the (Nafion)-stabilised ink (suspension) was deposited on its surface using a micro-syringe.

Before the electrochemical measurements, the electrolyte was deaerated by bubbling nitrogen gas for 20 min. The electrode was subjected to 20 cycles in the 0.2 to–0.9-V potential to clean the surface. Then, cathodic polarization curves were recorded in O_2-saturated 0.5 M NaOH solution by scanning the electrode potential at 5 $mV\,s^{-1}$ and different rotating speeds.

Characterization techniques

The morphology of oxides was examined using a JEOL (JSM-5600LV) scanning electron microscope. Room temperature X-ray diffraction patterns were collected using a Siemens D 500 diffractometer operating with a Co $K_{\alpha 1}$ (λ= 1.7889 Å) radiation.

The IR spectra were recorded between 400 and 1,400 cm^{-1} with a PERKIN ELMER FT-IR spectrum 1000 instrument, using the KBr pellet technique. Magnetic properties of the samples were investigated with conventional vibrating samples magnetometer at 5 K in a maximum field of 18 kOe.

Electrical resistivity ρ was measured using an Autolab PGSTAT30 at room temperature in air on compacted pellets (1 cm diameter) under a pressure of 5 t for 2 min using a hydraulic press. The pellets were then sintered at 1,150 °C during 2 h in a reducing atmosphere. In order to make the electrical contacts, conducting silver paints was applied on both sides of the pellets. The electrochemical and impedance experiments were performed using an Autolab PGSTAT. Impedance spectra were recorded in the 10^5 to the 10^{-2}-Hz range with an ac signal of 5 mV amplitude.

Results and discussion

XRD analysis

The purity of the samples and their crystallographic structure were investigated by X-ray diffraction (XRD). Figure 1 shows XRD patterns of the SFCMO compounds. They can all be indexed to a tetragonal double perovskite structure, with minor traces of impurity phases.

Results agree very well with the XRD patterns of the two parent compounds Sr_2FeMoO_6 (SFMO) and Sr_2CoMoO_6 (SCMO) reported, respectively, in the literature [17, 18]. Indeed, detailed inspection of the XRD data reveals that weak reflections attributed to Sr_2MoO_4, Sr_2FeO_{4-x} and Fe appear in the doped samples. As noticed, increase of Co produce peak broadening. These broader diffraction peaks most pronounced at large angles 2θ suggest smaller grain size for the Co-rich samples [19].

All the samples exhibit superstructure peaks (101) and (103) arising from the ordering of Fe/Mo and Co/Mo at B/B′ sites. It is well-known that such atomic order is apt to be disturbed, namely when Fe ions occupy the Mo site and vice versa. This is the so-called anti-site (AS) defect which is sensitive to substitution (x) of Fe with Co ions.

In the present case, the intensity of the superstructure reflexion (101) decreases with increasing Co content from x=0 to x=0.75. The degree of ordering is calculated on the relative intensity of the superstructure reflexion (101) peak. In the inset of Fig. 1, the depicted ratio $I_{(101)}/[I_{(112)}+I_{(200)}]$ decreases almost linearly as x increases. This indicates that Fe/Mo ordering is reduced and AS defect increases with increasing Co content. Any variation of the ratio is almost within the error bar of 5 %.

Figure 2 shows the field-dependent magnetization of SFCMO for different x measured at 5 K and in a maximum field of 18 kOe. All magnetization loops present a ferromagnetic-like shape, with small remanence and coercive field. Magnetization increases rapidly with external fields and then saturates to the value of saturated magnetization M_s. The magnetic moment systematically decreases with increasing x as shown in the inset of Fig. 2.

The estimated values of M_s are 3.3, 2.5, 1.5, 1.2 and 1 μ_B/f.u. for x=0, 0.25, 0.5, 0.75 and 1, respectively. A higher M_s for SFMO indicates a greater degree of order of the Fe and Mo atoms.

In order to calculate the anti-site defect concentration AS in SFCMO samples, we apply the following relation: M_s (x, AS)=(1−2 AS) (4+x). (1) For AS=0 (without disorder), the M_s increases with increasing x, and the ideal value is 4 μ_B/f.u. for x=0. However, the measured moment decreases with increasing x. This decrease can be caused by the anti-site defects and other effects such as the presence of oxygen vacancies [20, 21]. In Fig. 3a, we show the obtained AS values for each sample as a function of x. In agreement with the trend already observed from the $I_{(101)}/[I_{(112)}+I_{(200)}]$ variation, the increase of Co content induces larger disorder in the Fe/Mo sublattices and hence resulting in more anti-site defect concentration AS. The increase of AS may lead to a decrease of the electrical conductivity of the substituted SFMO samples as mentioned in our previous work [22] and as reported in literature [23].

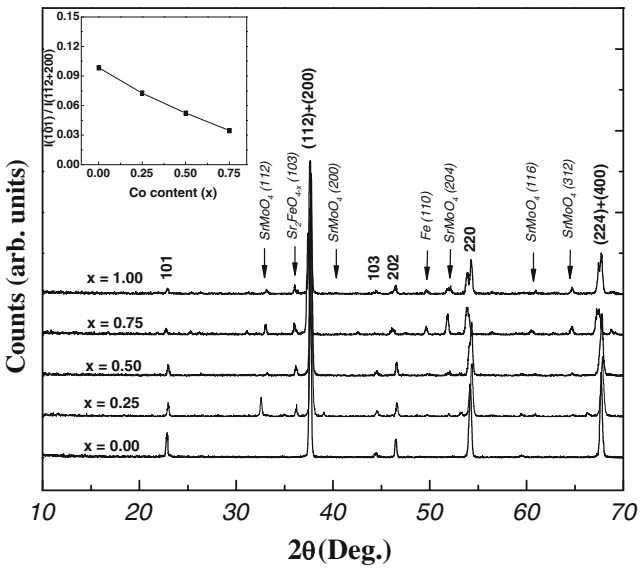

Fig. 1 X-ray diffraction patterns for $Sr_2Fe_{1-x}Co_xMoO_6$ ($0\leq\times\leq1$) samples with Co K_α radiation. *Inset* dependence of relative intensity ratio $I_{(101)}/[I_{(112)}+I_{(200)}]$ on the level of Co content x

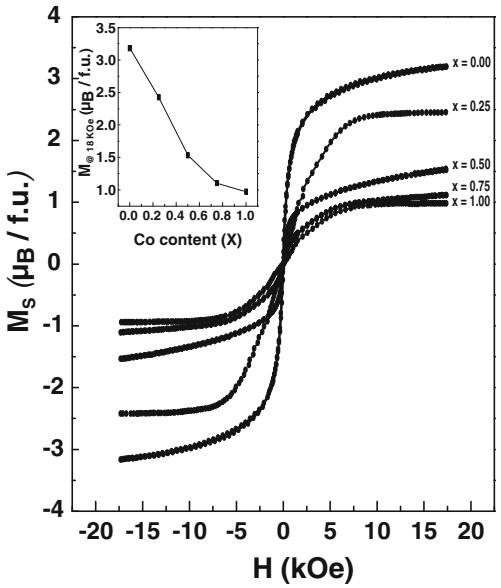

Fig. 2 Magnetization curves of $Sr_2Fe_{1-x}Co_xMoO_6$ ($0\leq\times\leq1$) at 5 K. *Inset* dependence of saturation magnetization on cobalt content x for $Sr_2Fe_{1-x}Co_xMoO_6$ ($0\leq\times\leq1$) at 5 K

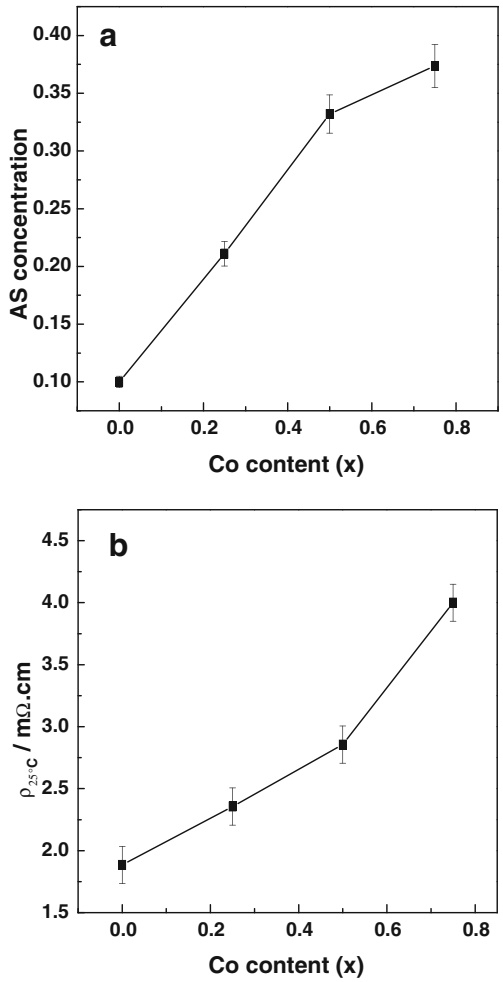

Fig. 3 Variation of **a** anti-site defect and **b** electrical resistivity ρ as a function of the Co content x for $Sr_2Fe_{1-x}Co_xMoO_6$ ($0 \leq \times \leq 0.75$)

Recently, Huang et al. [24] and Retuerto et al. [25] reported that pure ordered Sr_2FeMoO_6 double perovskite have been obtained using encapsulation technique under very low oxygen partial pressures and wet-chemistry technique, respectively. The homogeneous morphology and the high degree of Fe/Mo ordering are a consequence of the uniform mixing of starting reactants in an atomic scale. More recently, similar features have been also observed for Sr_2FeMoO_6 powders prepared by the polyacrylamide gel combustion synthesis [26] where a perfect cationic mixing at atomic level was promoted. Thus, the structural, transport, magnetic and electrochemical properties are strongly dependent on the synthesis procedure undertaken to prepare such compounds.

Electrical properties

The composition dependence of electrical resistivity ρ for the samples $Sr_2Fe_{1-x}Co_xMoO_6/C$ ($0 \leq \times \leq 0.75$) is shown in Fig. 3b. The value of ρ for the sample with $x=0$ (SFMO) is close to that reported by Zhang et al. [27] for the same composition prepared through a solid-state reaction. In substituted compounds, ρ increases notably by increasing the Co content x from $x=0$ to $x=0.75$. This is because of anti-site defects that increase the disorder (see Fig. 3a) leading to localization of the charge carriers, thus resulting in an increase in the electrical resistivity [28].

Oxide morphology and IR spectroscopy

In order to have some insight into the grain morphology of the oxides, SEM of two samples $x=0$ and $x=0.25$ are shown in Fig. 4. The $x=0.25$ sample exhibits relatively spherical and smaller grains with an average grain size of about 1.5–2 μm diameter (Fig. 4b), while the $x=0$ sample (SFMO) has grains that are much larger and connected to each other and with no well-defined shape (Fig. 4a). Addition of cobalt seems to act as a nucleation centre for the growth of the

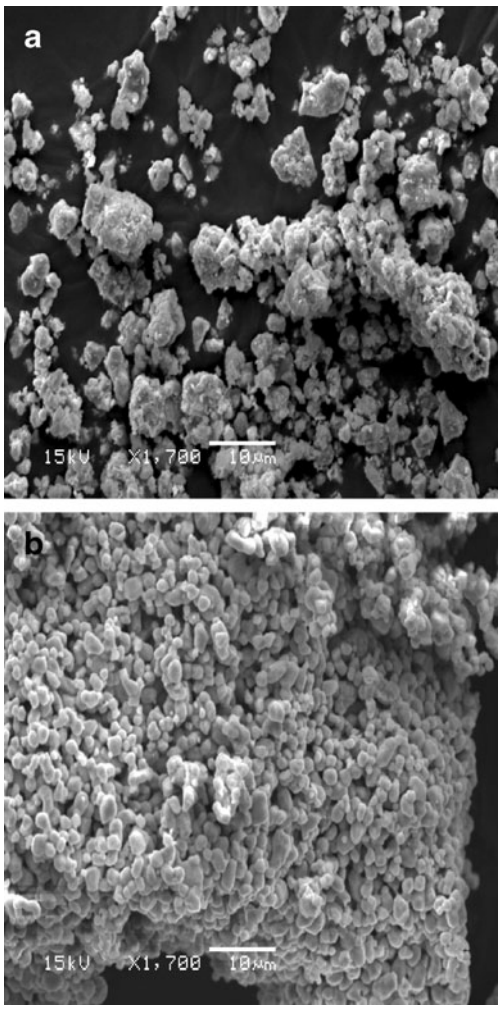

Fig. 4 SEM micrographs of $Sr_2Fe_{1-x}Co_xMoO_6$ (**a**) $x=0$ and (**b**) $x=0.25$ double perovskites sintered at 1,100 °C for 2 h in a stream of H_2/N_2 (5:95 %)

perovskite crystalline grains. As a Co amount is added to SFMO oxide, the number of such nucleation centres increases, which effectively raises the number of grains with small sizes.

Figure 5 displays the infrared spectra for $Sr_2Fe_{1-x}Co_x$-MoO_6 (x=0, 0.25, 0.5 and 0.75) oxides. All spectra are rather similar showing two absorption bands around 600 and 820 cm^{-1} and a weak band around 400 cm^{-1}. The weak band centred at about 600 cm^{-1} is attributed to Mo–O antisymmetric stretching mode of MoO_6 octahedra, and the relatively strong band at about 820 cm^{-1} is ascribed to Mo–O symmetric stretching mode [29]. The absorption band around 400 cm^{-1} is ascribed to Fe–O vibration mode of FeO_6 octahedra [30].

Oxygen reduction on SFCMO electrocatalysts

Linear voltammetry

To study the effect of rotation on catalytic activity, the current–potential curves recorded for oxygen reduction on thin layers of SCMO/C powder at five rotation rates (between 400 and 2,500 rpm) with a 5-$mV\,s^{-1}$ scan rate are presented in Fig. 6. The cathodic currents correspond to ORR because no current was observed under a nitrogen atmosphere. The ORR current density starts at about −0.15 V/Hg-HgO and shows one limiting current plateau at −0.4 V/Hg-HgO. The limiting current density i_{lim} increases markedly with increasing angular frequency ω.

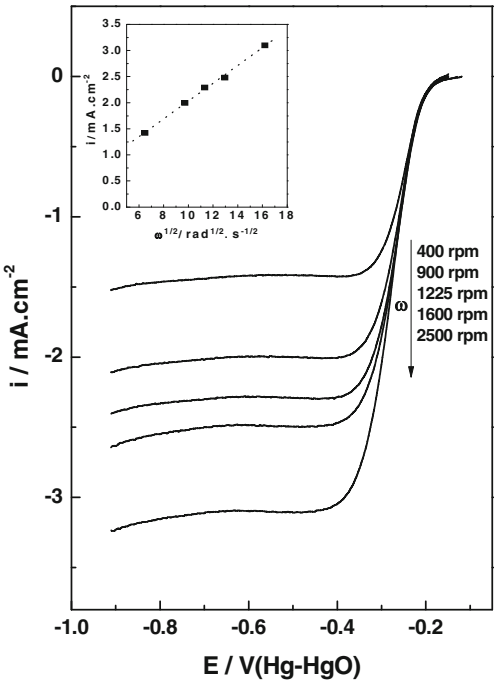

Fig. 6 Linear voltammetry curves for oxygen reduction on SCMO/C electrocatalyst. *Inset* Levich plot at −0.5 V/Hg-HgO collected on SCMO/C electrocatalyst in O_2–saturated 0.5 M NaOH solution at different rotation rates. Disk area, 0.07 cm^2

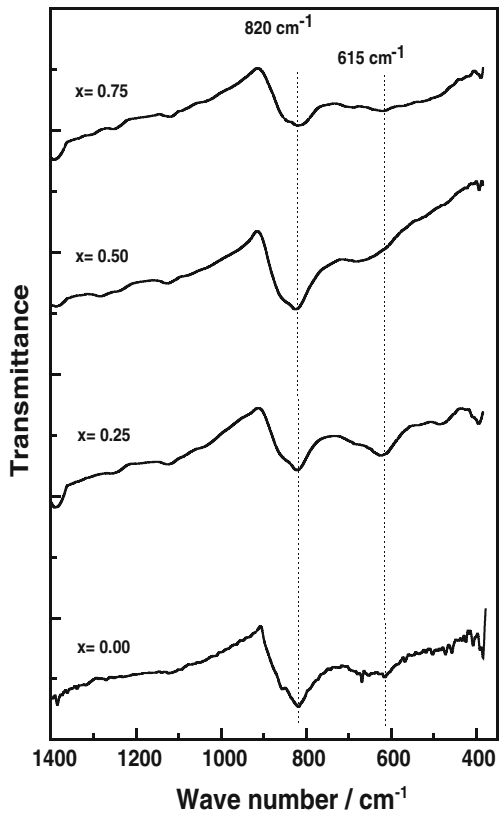

Fig. 5 Typical FT-IR spectra of the investigated $Sr_2Fe_{1-x}Co_xMoO_6$ compounds. From *bottom* to *top*, x=0, 0.25, 0.50 and 0.75

The i_{lim} for SCMO/C electrocatalyst, measured at −0.5 V/Hg-HgO, was plotted as a function of $\omega^{1/2}$ (inset of Fig. 6). A straight line was obtained, indicating that ORR is diffusion controlled [31]. From the slope of Levich plot, the diffusion coefficient of O_2 in 0.5 M NaOH and 25 °C was calculated according to the following relation:

$$B = 0.62nFC_{O_2}D_{O_2}{}^{2/3}\nu^{-1/6}, \quad (2)$$

where n is the number of electrons transferred per oxygen molecule, assumed to be 4, F is the Faraday constant (96,500 $C\,mol^{-1}$); C_{O_2} is the concentration of oxygen in 0.5 M NaOH ($0.843\times10^{-6}\,mol\,cm^2\,s^{-1}$); D_{O_2} is the diffusion coefficient of oxygen and ν is the kinematic viscosity of 0.5 M NaOH solution (9.784×10^{-3} $cm^2\,s^{-1}$) [32].

A value of $1.75\times10^{-4}\,A\,cm^2\,s^{-1/2}$ for the slope is obtained giving D_{O_2} at $0.25\times10^{-5}\,cm^2\,s^{-1}$ which is in the same order of magnitude as that of literature ($1.43\times10^{-5}\,cm^2\,s^{-1}$), reported in [33], thus providing evidence that the oxygen reduction occurs via a direct pathway of four-electron reduction to OH^-.

It is worth mentioning that the voltammograms for the $Sr_2Fe_{1-x}Co_xMoO_6/C$ ($0 \leq \times \leq 1$) electrocatalysts shown in Fig. 7 display different shapes. The compounds with $x=0$, 0.5 and 0.75 exhibit likely two plateaus due to the parallel occurrence of two- and four-electron oxygen reduction pathways while compounds with $x=0.25$ and $x=1$ show only one plateau. Determination of limiting current densities i_{lim} according to Levich relation for the four-electron and two-electron reduction processes is estimated to be 3.15 and 1.8 mA/cm^2, respectively. Comparison between the calculated and measured i_{lim} plateaus values reveals that they are close and indicates apparently a reduction of O_2 to HO_2^- and O_2 to OH^- on the first and second compound series, respectively. In the −0.4- to −0.8-V potential range, the dependence of the current density on the substitution degree x is also observed. Indeed, the higher the x, the lower the performance, i.e., observed small current densities. The SCMO/C compound ($x=1$) exhibits the best performance with the highest catalytic activity towards oxygen reduction, most of which is due to the direct four-electron reduction rather than the two-electron reduction to peroxide as demonstrated previously [12].

Figure 8 shows two Tafel slopes for $Sr_2Fe_{1-x}Co_xMoO_6/C$ ($0 \leq \times \leq 1$) electrocatalysts, the first one at low overpotentials (ca. −0.10 to −0.23 V/Hg-HgO), and the Tafel slope value is

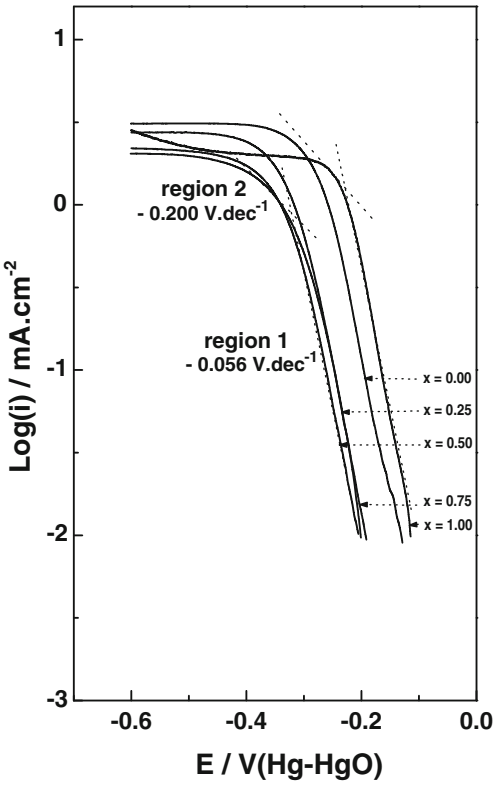

Fig. 8 Tafel plots of oxygen reduction on $Sr_2Fe_{1-x}Co_xMoO_6/C$ ($0 \leq \times \leq 1$) electrocatalysts in 0.5 M NaOH, sweep rate 5 mVs^{-1}, RDE at 2,500 rpm

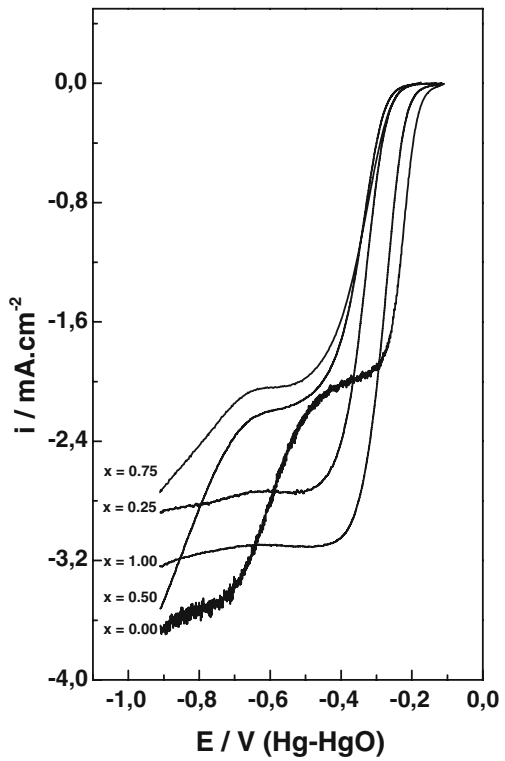

Fig. 7 Linear voltammetry curves for oxygen reduction on $Sr_2Fe_{1-x}Co_xMoO_6/C$ ($0 \leq \times \leq 1$) in O_2 saturated 0.5 M NaOH solution at 2,500 rpm. Disk area, 0.07 cm^2

about −0.056 Vdec^{-1}, while at high overpotentials (ca. < −0.30 V/Hg-HgO), it is about −0.20 Vdec^{-1}. According to reported Tafel behaviour for oxygen reduction, a similar transition occurring with Pt [34] and Ru [35] electrodes from −0.06 and −0.08 to −0.20 and −0.18 Vdec^{-1}, respectively, is reasonably well-understood. Also a value of −0.047 Vdec^{-1} at lower overpotentials was obtained on $La_{1-x}Sr_xMnO_3$ perovskites [36].

Steady-state polarization

The ORR on carbon supported SFCMO compounds in 0.5 M NaOH solution was also investigated by plotting current–potential curves in the steady-state regime. The time taken for the current to reach a steady state was found to vary with the applied potential: It was about 5 min at high over-potentials and about 10 min at low overpotentials. Figure 9 shows the steady-state polarization plots for the SFCMO/C electrocatalysts, Carbon (Vulcan XC-72). For comparison, the behaviour under the same conditions of a Pt foil is also included. The small currents observed for the GC substrate indicate that it is a relatively inactive material. The polarization curves reveal that the electrocatalytic activity decreases with increasing x from 0 to 0.75 and that the

highest activity towards oxygen reduction was observed for Sr_2CoMoO_6/C and $Sr_2Fe_{0.75}Co_{0.25}MoO_6$ for which this activity is ascribed, as mentioned above, to the four-electron reduction pathway providing higher limiting currents. As there is parallel evolution established for the electrochemical activity and the electrical resistivity [36], the decrease of the cathodic current densities, expressing this activity, with increasing cobalt content x may be attributed to the increased disorder in Fe/Mo sub-lattice and therefore to the increased resistivity as shown above. In addition, the tiny amount of $SrMoO_4$ visible in the XRD data (Fig. 1), which is induced to appear at the grain boundaries of the compounds as insulating impurity phase [37], could also be responsible for the decrease of the resistivity, with a consequential drop in the electrochemical activity.

Electrochemical impedance study

To provide evidence of O_2 diffusion process occurring at the interface, using electrochemical impedance spectroscopy technique, Nyquist diagrams obtained potentiostatically with RDE system for O_2 reduction on SCMO/C at −0.6 V/Hg-HgO and different rotation rates were plotted (Fig. 10). According to the result reported previously [12], the diagrams show a large capacitive loop consisting of two overlapping loops. The first masked loop in the high-frequency range is due to charge transfer process of oxygen reduction at the electrode/electrolyte interface. It is noteworthy that while the first loop remains constant, the diffusion loop size over the whole rotation rates ω range investigated shows a clear decrease with the increase of ω. This suggests that

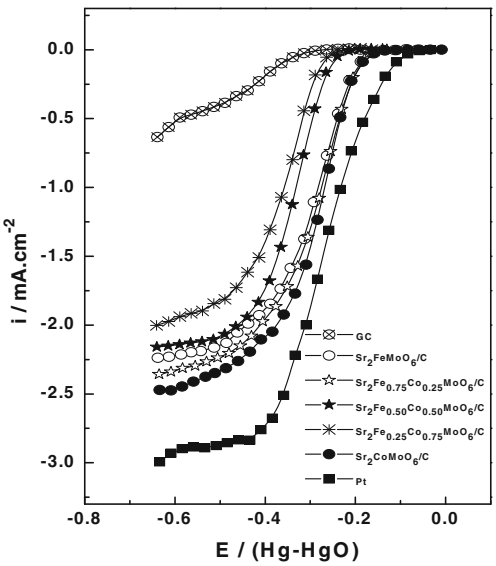

Fig. 9 Steady state polarization plots of oxygen reduction on $Sr_2Fe_{1-x}Co_xMoO_6/C$ ($0 \le \times \le 1$) electrocatalysts in O_2-saturated 0.5 M NaOH solution at 2,500 rpm. Disk area, 0.07 cm^2

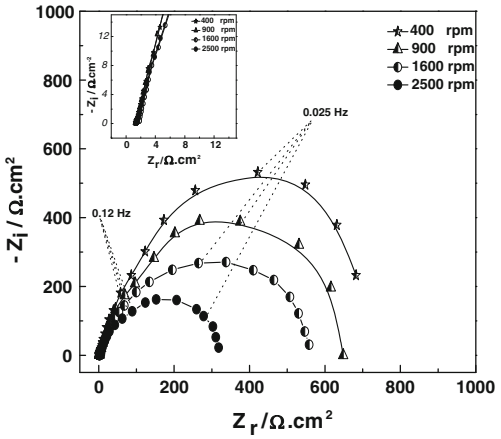

Fig. 10 Nyquist plots for O_2 reduction on SCMO/C in O_2-satured 0.5 M NaOH solution at 400, 900, 1,600 and 2,500 rpm at −0.6 V/Hg-HgO and 25 °C

ORR is limited by the diffusion of molecular oxygen from the bulk of the electrolyte to the electrode surface. In the inset of Fig. 10, an electrolyte resistance of about 1.5 Ωcm^2 was determined for different rotation rates.

The characterization of the ORR on the $Sr_2Fe_{1-x}Co_xMoO_6/C$ electrocatalysts was carried out at −0.6 V/Hg-HgO on a RDE at 2,500 rpm. The Nyquist diagrams plotted in Fig. 11 showing the same shape for all compositions x correspond mainly to diffusion limitation for the ORR. In accordance with the limiting current evolution observed on the polarization curves for the $Sr_2Fe_{1-x}Co_xMoO_6/C$ ($0 \le \times \le 0.75$), the diffusion loop size increases strongly with increasing the Co content x, confirming the decrease of the electrochemical performance of the substituted samples. This behaviour may be understood based once again on the increase of the anti-site concentration, i.e. increased disorder in Fe/Mo sub-lattice shown above.

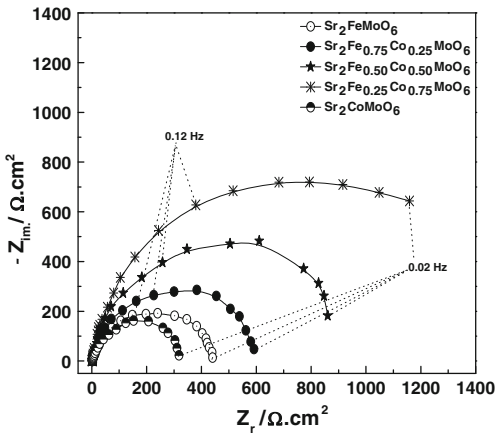

Fig. 11 Nyquist plots for O_2 reduction on $Sr_2Fe_{1-x}Co_xMoO_6/C$ ($0 \le \times \le 1$) in 0.5 M NaOH at −0.6 V/Hg-HgO and 2,500 rpm

Conclusion

The effect of Co substitution for Fe in Sr_2FeMoO_6 mixed with carbon (Vulcan XC-72) on the electrocatalytic properties for oxygen reduction in alkaline medium has been investigated. The structural study for the compounds indicates that all intense diffraction peaks can be indexed according to a double perovskites structure with tetragonal I4/mmm symmetry and that Sr_2MoO_4, Sr_2FeO_{4-x} and Fe appear in the doped samples as minor impurities. Co substitution for Fe causes an increase of the AS defects and leads to an increase of the number of nucleation centres. This nucleation raises the number of grains with small sizes. Resistivity ρ of substituted compounds is higher than the parent one. The increase of ρ with Co content could be attributed to the effect of increasing the Fe/Mo disorder. Within the studied electrocatalysts, it was observed that the electrocatalyst with x=0.75 shows the minimum catalytic activity towards oxygen reduction. The decrease in activity with increasing x up to 0.75 can be ascribed to the increase of resistivity which becomes in fact the determinant of the ORR process. The SCMO/C compound (x=1) having its own electrical properties exhibits the best performance with the highest catalytic activity towards oxygen reduction, most of which is due to the preferred direct four-electron reduction rather than the parasitic two-electron reduction to peroxide. Overall, the performance of the best compound in this series is still inferior to that of Pt electrode. Nevertheless, this limitation may be acceptable given the much lower cost of double perovskite-based catalysts. Future work will be undertaken to improve the electrical properties of the carbon/double perovskite composite by optimizing the electrode loading.

References

1. Meadowcroft DB (1970) Nature 226:847
2. Van Buren FR, Broers GHJ, Boesveld C, Bouman AJ (1978) J Electroanal Chem 87:381
3. Karlsson G (1985) Electrochim Acta 30:1555
4. Shimizu Y, Uemura K, Mastuda H, Miura N, Yamaoze N (1990) J Electrochem Soc 137:3430
5. Hammouche A, Kahoul A, Sauer DU, De Doncker RW (2006) J Power Sources 153:239
6. Vielstich W, Lamm A (2003) Handbook of fuel cells—fundamentals, technology and applications. Wiley, New York
7. Yamazoe N, Teraoka Y (1990) Catal Today 8:175
8. Wang X, Sui Y, Yang Q, Cheng J, Qian Z, Liu Z, Su W (2007) J Alloys Compd 431:6
9. Azad AK, Khan A, Eriksson SG, Irvine JTS (2009) Mater Res Bull 44:2181
10. Feng XM, Rao GH, Liu GY, Yang HF, Liu WF, Ouyang ZW, Yang LT, Liu ZX, Yu RC, Jin CQ, Liang JK (2002) J Phys Condens Matter 14:12503
11. Sher F, Venimaldhav A, Blamire MG, Dabrowski B, Kolesnik S, Attfield JP (2005) Solid State Sci 7:912
12. Cheriti M, Kahoul A (2012) Mater Res Bull 47:135
13. Huang YH, Liang G, Croft M, Lehtimäki M, Karppinen M, Goodenough JB (2009) Chem Mater 21:2319
14. Xue J, Shen Y, He T (2011) J Power Sources 196:3729
15. Yuan CL, Zhu Y, Ong PP, Shen ZX, Ong CK (2004) Solid State Commun 129:551
16. Fang TT, Wu MS, Ko TF (2001) J Mater Sci Lett 20:1609
17. Dinia A, Vénuat J, Colis S, Pourroy G (2004) Catal Today 89:297
18. Viola MC, Martinez-Lope MJ, Alonso JA, Velsco P, Martinez JL, Pedregasa JC, Carbonio RE, Fernandez-Diaz MT (2002) Chem Mater 14:812
19. Blasco J, Ritter C, Morellon L, Algarabel PA, De Teresa JM, Serrate D, García J, Ibarra MR (2002) Solid State Sci 4:651
20. Ogale AS, Ogale SB, Ramesh R, Venkatesan T (1999) Appl Phys Lett 75:537
21. Balcells LI, Navarro J, Bibes M, Roig A, Martinez B, Fontcuberta J (2001) Appl Phys Lett 78:781
22. Kahoul A, Azizi A, Colis S, Stoeffler D, Moubah R, Schmerber G, Leuvrey C, Dinia A (2008) J Appl Phys 104:123903
23. Zhang Q, Rao GH, Dong HZ, Xiao YG, Feng XM, Liu GY, Zhang Y, Liang JK (2005) Physica B 370:228
24. Huang YH, Lindén J, Yamouchi H, Karpinnen M (2004) Chem Mater 16:4337
25. Retuerto M, Alonso JA, Martínez-Lope MJ, Martínez JL, García-Hernández M (2004) Appl Phys Lett 85:266
26. Calleja A, Capdevila XG, Segarra M, Frontera C, Espiell F (2011) J Eur Ceram Soc 31:121
27. Zhang L, Zhou Q, He Q, He T (2010) J Power Sources 195:6356
28. Gaur A, Varma GD, Singh HK (2008) J Alloys Compd 460:581
29. Lavat AE, Baran EJ (2003) Vib Spectrosc 32:167
30. Zhai YQ, Qiao J, Qiu MD (2012) E-J Chem 9:818
31. Bard AJ, Faulkner LR (2001) Electrochemical methods, fundamentals and applications, 2nd edn. Wiley, New York
32. Lide DR (2010) Handbook of chemistry and physics, 90th edn. CRC, Boca Raton
33. Geniès L, Faure R, Durand R (1998) Electrochim Acta 44:1317
34. Yu EH, Scott K, Reeve RW (2003) Fuel Cells 3:169
35. Marković NM, Ross PN (1994) J Electrochem Soc 141:2590
36. Matsumoto Y, Yoneyama H, Tamura H (1977) J Electroanal Chem 83:237
37. Niebieskikwiat D, Caneiro A, Sánchez RD, Fontcuberta J (2001) Phys Rev B 64:180406